4

Calculation of Emitted Spectrum

4.1 Introduction

The radiation emitted by each element of volume in a gaseous nebula depends upon the abundances of the elements, determined by the previous evolutionary history of the gas, and on the local ionization, density, and temperature, determined by the radiation field and the abundances as described in the preceding two chapters. The most prominent spectral features are the emission lines, and many of these are the collisionally excited lines described in the preceding chapter on thermal equilibrium. The formalism developed there to calculate the cooling rate, and thus the thermal equilibrium, may be taken over unchanged to calculate the strength of these lines. If we could observe all the lines in the entire spectral region from the extreme ultraviolet to the far infrared, we could measure directly the cooling rate at each observed point in the nebula. Many of the most important lines in the cooling, for instance [O II] $\lambda\lambda 3726$, 3729 and [O III] $\lambda\lambda 4959$, 5007, are in the optical region and are easily measured. Other lines that are also important in the cooling, such as [O III] $2p^2\,^3P_0$–$2p^2\,^3P_1\,\lambda 88.4\,\mu$m, and $^3P_1$–$^3P_2 \lambda 51.8\mu$m, are in the far infrared region, while still others, such as C IV $\lambda\lambda 1548$, 1551, are in the vacuum ultraviolet.

For historical reasons, astronomers tend to refer to the chief emission lines of gaseous nebulae as *forbidden* lines. Actually, it is better to think of the bulk of the lines as *collisionally excited* lines, which arise from levels within a few volts of the ground level, and which therefore can be excited by collisions with thermal electrons. In fact, in the ordinary optical region all these collisionally excited lines are forbidden lines, because in the abundant ions all the excited levels within a few volts of the ground level arise from the same electron configuration as the ground level itself, and thus radiative transitions are forbidden by the parity selection rule. However, at wavelengths just slightly below the ultraviolet cutoff of the Earth's atmosphere, collisionally excited lines begin to appear that are not forbidden lines. Among others, many nebulae have strong permitted lines of Mg II $3s\,^2S$–$3p\,^2P^o\,\lambda\lambda 2796$, 2803, C IV $2s\,^2S$–$2p\,^2P^o\lambda\lambda 1548$, 1551, and Si IV $3s\,^2S$–$3p\,^2P^o\,\lambda\lambda 1394$, 1403.

In addition to the collisionally excited lines, the recombination lines of H I, He I, and He II are characteristic features of the spectra of gaseous nebulae. They are

emitted by atoms undergoing radiative transitions in cascading down to the ground level following recombinations to excited levels. In the remainder of this chapter, these recombination emission processes will be discussed in more detail. Finally, the continuum-emission processes, which are the bound–free and free–free analogues of the bound–bound transitions emitted in the recombination-line spectrum, will be examined.

4.2 Optical Recombination Lines

The recombination-line spectrum of H I is emitted by H atoms that have been formed by captures of electrons into excited levels and that are cascading by downward radiative transitions to the ground level. In the limit of very low density, the only processes that need be considered are captures and downward-radiative transitions. Thus the equation of statistical equilibrium for any level nL may be written

$$n_p n_e \alpha_{nL}(T) + \sum_{n'>n}^{\infty} \sum_{L'} n_{n'L'} A_{n'L',nL} = n_{nL} \sum_{n''=1}^{n-1} \sum_{L''} A_{nL,n''L''}. \tag{4.1}$$

Note in general $A_{n'L',n''L''} \neq 0$ only if $L' = L'' \pm 1$.

It is convenient to express the population in terms of the dimensionless factors b_{nL} that measure the deviation from thermodynamic equilibrium at the local T, n_e, and n_p. In thermodynamic equilibrium the Saha equation

$$\frac{n_p n_e}{n_{1S}} = \left(\frac{2\pi mkT}{h^2}\right)^{3/2} \exp(-h\nu_0/kT), \tag{4.2}$$

and the Boltzmann equation

$$\frac{n_{nL}}{n_{1S}} = (2L+1)\exp(-\chi_n/kT), \tag{4.3}$$

apply. The factor $2L+1$ is the ratio of statistical weights of the nL and $1S$ levels. Then the population in the level nL in thermodynamic equilibrium may be written

$$n_{nL} = (2L+1)\left(\frac{h^2}{2\pi mkT}\right)^{3/2} \exp(X_n/kT) n_p n_e, \tag{4.4}$$

where

$$X_n = h\nu_0 - \chi_n = \frac{h\nu_0}{n^2} \tag{4.5}$$

is the ionization potential of the level nL. Therefore, in general, the population may be written

$$n_{nL} = b_{nL}(2L+1)\left(\frac{h^2}{2\pi mkT}\right)^{3/2} \exp(X_n/kT) n_p n_e, \tag{4.6}$$

and $b_{nL} = 1$ in thermodynamic equilibrium.

Substituting this expression in (4.1),

$$\alpha_{nL} \frac{1}{(2L+1)} \left(\frac{2\pi mkT}{h^2}\right)^{3/2} \exp(-X_n/kT)$$
$$+ \sum_{n'>n}^{\infty} \sum_{L''} b_{n'L'} A_{n'L',nL} \left(\frac{2L'+1}{2L+1}\right) \exp\left[(X_{n'} - X_n)/kT\right] \tag{4.7}$$
$$= b_{nL} \sum_{n''=1}^{n-1} \sum_{L''} A_{nL,n''L''},$$

it can be seen that the b_{nL} factors are independent of density as long as recombination and downward-radiative transitions are the only relevant processes. Furthermore, it can be seen that the Equations (4.7) can be solved by a systematic procedure working downward in n, for if the b_{nL} are known for all $n \geq n_K$, then the n Equations (4.7), with $L = 0, 1, \ldots, n-1$ for $n = n_{K-1}$, each contain a single unknown b_{nL} and can be solved immediately, and so on successively downward.

It is convenient to express the solutions in terms of the cascade matrix $C(nL, n'L')$, which is the probability that population of nL is followed by a transition to $n'L'$ via all possible cascade routes. The cascade matrix can be generated directly from the probability matrix $P(nL, n'L')$, which gives the probability that population of the level nL is followed by a direct radiative transition to $n'L'$,

$$P_{nL,n'L'} = \frac{A_{nL,n'L'}}{\displaystyle\sum_{n''=1}^{n-1}\sum_{L''} A_{nL,n''L''}} \tag{4.8}$$

which is zero unless $L' = L \pm 1$.

Hence, for $n' = n - 1$,

$$C_{nL,n-1L'} = P_{nL,n-1L'};$$

for $n' = n - 2$,

$$C_{nL,n-2L'} = P_{nL,n-2L'} + \sum_{L''=L'\pm1} C_{nL,n-1L''} P_{n-1L'',n-2L'};$$

and for $n' = n - 3$,

$$C_{nL,n-3L'} = P_{nL,n-3L'}$$
$$+ \sum_{L''=L'\pm 1} \left[C_{nL,n-1L''} P_{n-1L'',n-3L'} + C_{nL,n-2L''} P_{n-2L'',n-3L'} \right]$$

so that if we define

$$C_{nL,nL''} = \delta_{LL''}, \tag{4.9}$$

then in general

$$C_{nL,n'L'} = \sum_{n''>n'}^{n} \sum_{L''=L'\pm 1} C_{nL,n''L''} P_{n''L'',n'L'}. \tag{4.10}$$

The solutions of the equilibrium Equations (4.1) may be immediately written down, for the population of any level nL is fixed by the balance between recombinations to all levels $n' \geq n$ that lead by cascades to nL and downward radiative transitions from nL:

$$n_p n_e \sum_{n'=n}^{\infty} \sum_{L'=0}^{n'-1} \alpha_{n'L'}(T) \, C_{n'L',nL} = n_{nL} \sum_{n''=1}^{n-1} \sum_{L''=L\pm 1} A_{nL,n''L'}. \tag{4.11}$$

It is convenient to express the results in this form because once the cascade matrix has been calculated, it can be used to find the b_{nL} factors or the populations n_{nL} at any temperature, or even for cases in which the population occurs by other non-radiative processes, such as collisional excitation from the ground level or from an excited level. To carry out the solutions, it can be seen from (4.11) that it is necessary to fit series in n, n', L, and L' to $C_{nL,n'L'}$ and α_L, (T), and extrapolate these series as $n \to \infty$. Once the populations n_{nL} have been found, it is simple to calculate the emission coefficient in each line:

$$j_{nn'} = \frac{h\nu_{nn'}}{4\pi} \sum_{L=0}^{n-1} \sum_{L'=L\pm 1} n_{nL} A_{nL,n'L'}. \tag{4.12}$$

The situation we have been considering is commonly called Case A in the theory of recombination-line radiation, and assumes that all line photons emitted in the nebula escape without absorption and therefore without causing further upward transitions. Case A is thus a good approximation for gaseous nebulae that are optically thin in all H I resonance lines, but in fact such nebulae can contain only a relatively small amount of gas and are mostly too faint to be easily observed.

Nebulae that contain observable amounts of gas generally have quite large optical depths in the Lyman resonance lines of H I. This can be seen from the equation for the central line-absorption cross section,

$$a_0(\text{L}n) = \frac{3\lambda_{n1}^3}{8\pi} \left(\frac{m_\text{H}}{2\pi kT} \right)^{1/2} A_{nP,1S} \, [\text{cm}^2], \tag{4.13}$$

where λ_{n1} is the wavelength of the line. Thus, at a typical temperature $T = 10,000$ K, the optical depth in Lα is about 10^4 times the optical depth at the Lyman limit $\nu = \nu_0$ of the ionizing continuum, and an ionization-bounded nebula with $\tau_0 \approx 1$ therefore has $\tau(\text{L}\alpha) \approx 10^4$, $\tau(\text{L}\beta) \approx 10^3$, $\tau(\text{L}8) \approx 10^2$, and $\tau(\text{L}18) \approx 10$. In each scattering there is a finite probability that the Lyman-line photon will be converted to a lower-series photon plus a lower member of the Lyman series. Thus, for instance, each time an Lβ photon is absorbed by an H atom, raising it to the $3 \, ^2P$ level, the probability that this photon is scattered is $P_{31,10} = 0.882$, while the probability that it is converted to Hα is $P_{31,20} = 0.118$, so after nine scatterings an average Lβ photon is converted to Hα (plus two photons in the $2 \, ^2S \to 1 \, ^2S$ continuum) and cannot escape from the nebula. Likewise, an average Lγ photon is transformed, after a relatively few scatterings, either into a Pα photon plus an Hα photon plus an Lα photon, or into an Hβ photon plus two photons in the $2 \, ^2S$–$1 \, ^2S$ continuum. Thus, for these large optical depths, a better approximation than Case A is the opposite assumption that every Lyman-line photon is scattered many times and is converted (if $n \geq 3$) into lower-series photons plus either Lα or two-continuum photons. This large optical depth approximation is called Case B, and is more accurate than Case A for most nebulae. However, it is clear that the real situation is intermediate, and is similar to Case B for the lower Lyman lines, but progresses continuously to a situation nearer Case A as $n \to \infty$ and $\tau(\text{L}n) \to 1$.

Under Case B conditions, any photon emitted in an $n \, ^2P^o \to 1 \, ^2S$ transition is immediately absorbed nearby in the nebula, thus populating the n^2P^o level in another atom. Hence, in Case B, the downward radiative transitions to $1 \, ^2S$ are simply omitted from consideration, and the sums in the equilibrium Equations (4.1), (4.7), (4.8), and (4.11) are terminated at $n'' = n_0 = 2$ instead of at $n_0 = 1$ as in Case A. The detailed transition between Cases A and B will be discussed in Section 4.5.

Selected numerical results from the recombination spectrum of H I are listed in Tables 4.1 and 4.2 for Cases A and B, respectively. Note that, in addition to the emission coefficient $j_{42} = j_{\text{H}\beta}$ and the relative intensities of the other lines, it is also sometimes convenient to use the effective recombination coefficient, defined by

$$n_p n_e \alpha_{nn'}^{eff} = \sum_{L=0}^{n-1} \sum_{L'=L\pm 1} n_{nL} A_{nL,n'L'} = \frac{4\pi j_{nn'}}{h\nu_{nn'}}. \tag{4.14}$$

Table 4.1

H I recombination lines (Case A, low-density limit)

	T			
	2,500 K	5,000 K	10,000 K	20,000 K
$4\pi j_{H\beta}/n_e n_p$ (erg cm^3 s^{-1})	2.70×10^{-25}	1.54×10^{-25}	8.30×10^{-26}	4.21×10^{-26}
$\alpha_{H\beta}^{eff}$ (cm^3 s^{-1})	6.61×10^{-14}	3.78×10^{-14}	2.04×10^{-14}	1.03×10^{-14}
Balmer-line intensities relative to Hβ				
$j_{H\alpha}/j_{H\beta}$	3.42	3.10	2.86	2.69
$j_{H\gamma}/j_{H\beta}$	0.439	0.458	0.470	0.485
$j_{H\delta}/j_{H\beta}$	0.237	0.250	0.262	0.271
$j_{H\varepsilon}/j_{H\beta}$	0.143	0.153	0.159	0.167
$j_{H8}/j_{H\beta}$	0.0957	0.102	0.107	0.112
$j_{H9}/j_{H\beta}$	0.0671	0.0717	0.0748	0.0785
$j_{H10}/j_{H\beta}$	0.0488	0.0522	0.0544	0.0571
$j_{H15}/j_{H\beta}$	0.0144	0.0155	0.0161	0.0169
$j_{H20}/j_{H\beta}$	0.0061	0.0065	0.0068	0.0071
Lyman-line intensities relative to Hβ				
$j_{L\alpha}/j_{H\beta}$	33.0	32.5	32.7	34.0
Paschen-line intensities relative to Hβ				
$j_{P\alpha}/j_{H\beta}$	0.684	0.562	0.466	0.394
$j_{P\beta}/j_{H\beta}$	0.267	0.241	0.216	0.196
$j_{P\gamma}/j_{H\beta}$	0.134	0.126	0.118	0.110
$j_{P8}/j_{H\beta}$	0.0508	0.0497	0.0474	0.0452
$j_{P10}/j_{H\beta}$	0.0258	0.0251	0.0239	0.0228
$j_{P15}/j_{H\beta}$	0.00750	0.00721	0.00691	0.00669
$j_{P20}/j_{H\beta}$	0.00310	0.00300	0.00290	0.00280

For hydrogen-like ions of nuclear charge Z, all the transition probabilities $A_{nL,n'L'}$ are proportional to Z^4, so the $P_{nL,n'L'}$, and $C_{nL,n'L'}$ matrices are independent of Z. The recombination coefficients α_{nL} scale as

$$\alpha_{nL}(Z, T) = Z \alpha_{nL}(1, T/Z^2);$$

the effective recombination coefficients scale in this same way, and since the energies $h\nu_{nn'}$ scale as

$$\nu_{nn'}(Z) = Z^2 \nu_{nn'}(1),$$

Table 4.2

H I recombination lines (Case B, low-density limit)

	T			
	2,500 K	5,000 K	10,000 K	20,000 K
$4\pi j_{H\beta}/n_e n_p$ (erg cm^3 s^{-1})	3.72×10^{-25}	2.20×10^{-25}	1.24×10^{-25}	6.62×10^{-26}
$\alpha_{H\beta}^{eff}$ (cm^3 s^{-1})	9.07×10^{-14}	5.37×10^{-14}	3.03×10^{-14}	1.62×10^{-14}
Balmer-line intensities relative to Hβ				
$j_{H\alpha}/j_{H\beta}$	3.30	3.05	2.87	2.76
$j_{H\gamma}/j_{H\beta}$	0.444	0.451	0.466	0.474
$j_{H\delta}/j_{H\beta}$	0.241	0.249	0.256	0.262
$j_{H\varepsilon}/j_{H\beta}$	0.147	0.153	0.158	0.162
$j_{H8}/j_{H\beta}$	0.0975	0.101	0.105	0.107
$j_{H9}/j_{H\beta}$	0.0679	0.0706	0.0730	0.0744
$j_{H10}/j_{H\beta}$	0.0491	0.0512	0.0529	0.0538
$j_{H15}/j_{H\beta}$	0.0142	0.0149	0.0154	0.0156
$j_{H20}/j_{H\beta}$	0.0059	0.0062	0.0064	0.0065
Paschen-line intensities relative to Hβ				
$j_{P\alpha}/j_{H\beta}$	0.528	0.427	0.352	0.293
$j_{P\beta}/j_{H\beta}$	0.210	0.187	0.165	0.146
$j_{P\gamma}/j_{H\beta}$	0.1060	0.0991	0.0906	0.0820
$j_{P\varepsilon}/j_{H\beta}$	0.0410	0.0392	0.0368	0.0343
$j_{P10}/j_{H\beta}$	0.0207	0.0199	0.0185	0.0172
$j_{P15}/j_{H\beta}$	0.00589	0.00571	0.00530	0.00501
$j_{P20}/j_{H\beta}$	0.00240	0.00240	0.00220	0.00210
Brackett-line intensities relative to Hβ				
$j_{Br\alpha}/j_{H\beta}$	0.1447	0.1091	0.0834	0.0640
$j_{Br\beta}/j_{H\beta}$	0.0709	0.0578	0.0471	0.0380
$j_{Br\gamma}/j_{H\beta}$	0.0387	0.0332	0.0281	0.0237
$j_{Br\delta}/j_{H\beta}$	0.0248	0.0216	0.0186	0.0157
$j_{Br10}/j_{H\beta}$	0.01193	0.01065	0.00920	0.00796
$j_{Br15}/j_{H\beta}$	0.00317	0.00295	0.00263	0.00231
$j_{Br20}/j_{H\beta}$	0.00127	0.00124	0.00109	0.00097

the emission coefficient is

$$j_{nn'}(Z, T) = Z^3 j_{nn'}(1, T/Z^2). \tag{4.15}$$

Thus the calculations for H I at a temperature T can also be applied to He II at $T' = 4T$. In Table 4.3 some of the main features of the He II recombination line spectrum are listed for Case B, with the strongest line in the optical spectrum, $\lambda 4686$ ($n = 4 \rightarrow 3$), as the reference line. Note that the Fowler series ($n \rightarrow 3$) except for $\lambda 4686$ and $\lambda 3203$, and the entire "Balmer" series ($n \rightarrow 2$) are in the vacuum ultraviolet spectral region.

Next let us return to the H I recombination lines and examine the effects of collisional transitions at finite nebular densities. The largest collisional cross sections involving the excited levels of H are for transitions $nL \rightarrow nL \pm 1$ which have essentially zero energy difference. Collisions with both electrons and protons can cause these angular-momentum-changing transitions, but because of the small energy difference, protons are more effective than electrons; for instance, representative values of the mean cross sections for thermal protons at $T \approx 10,000$ K are $\sigma(2\ ^2S \rightarrow 2\ ^2P^o) \approx 3 \times 10^{-10}$ cm^2, $\sigma(10\ ^2L \rightarrow 10\ ^2L \pm 1) \approx 4 \times 10^{-7}$ cm^2, and $\sigma(20\ ^2L \rightarrow 20\ ^2L \pm 1) \approx 6 \times 10^{-6}$ cm^2. (Both of the latter are evaluated for $L \approx n/2$.) These collisional transitions must then be included in the equilibrium equations, which are modified from (4.1) to read

$$n_p n_e \alpha_{nL}(T) + \sum_{n'>n}^{\infty} \sum_{L'=L\pm 1} n_{n'L'} A_{n'L',nL} + \sum_{L'=L\pm 1} n_{n'L'} n_p q_{nL',nL}$$
$$= n_{nL} \left[\sum_{n''=n_0}^{n-1} \sum_{L''=L\pm 1} A_{nL,n''L''} + \sum_{L''=L\pm 1} n_p q_{nL,nL''} \right] \tag{4.16}$$

where $n_0 = 1$ or 2 for Cases A and B, respectively, and

$$q_{nL,n'L'} \equiv q_{nL,n'L'}(T) = \int_0^{\infty} u \sigma(nL \rightarrow n'L') f(u)\, du \ [\text{cm}^3\ \text{s}^{-1}] \tag{4.17}$$

is the collisional transition probability per proton per unit volume. For sufficiently large proton densities, the collisional terms dominate, and because of the principle of detailed balancing, they tend to set up a thermodynamic equilibrium distribution of the various L levels within each n; that is, they tend to make the populations proportional to the statistical weights,

$$\frac{n_{nL}}{n_{nL'}} = \frac{\omega_{nL}}{\omega_{nL'}} = \frac{(2L+1)}{(2L'+1)}$$

Table 4.3

He II recombination lines (Case B, low-density limit)

	T			
	5,000 K	10,000 K	20,000 K	40,000 K
$4\pi j_{\lambda 4686}/n_e n_{He^{++}}$ (erg cm^3 s^{-1})	3.14×10^{-24}	1.58×10^{-24}	7.54×10^{-25}	3.48×10^{-25}
$\alpha_{H\beta}^{eff}$ (cm^3 s^{-1})	7.40×10^{-13}	3.72×10^{-13}	1.77×10^{-13}	8.20×10^{-14}
"Balmer"-line ($n \rightarrow 2$) intensities relative to $\lambda 4686$				
$j_{32}/j_{\lambda 4686}$	5.60	6.25	7.14	8.15
$j_{42}/j_{\lambda 4686}$	1.54	1.89	2.34	2.84
$j_{52}/j_{\lambda 4686}$	0.66	0.84	1.06	1.32
$j_{72}/j_{\lambda 4686}$	0.22	0.28	0.36	0.45
$j_{10,2}/j_{\lambda 4686}$	0.07	0.09	0.12	0.15
Fowler-line intensities ($n \rightarrow 3$) relative to $\lambda 4686$				
$j_{53}/j_{\lambda 4686}$	0.355	0.398	0.438	0.469
$j_{63}/j_{\lambda 4686}$	0.173	0.201	0.232	0.257
$j_{83}/j_{\lambda 4686}$	0.065	0.078	0.092	0.104
$j_{10,3}/j_{\lambda 4686}$	0.033	0.039	0.047	0.052
Pickering-line ($n \rightarrow 4$) intensities relative to $\lambda 4686$				
$j_{54}/j_{\lambda 4686}$	0.295	0.274	0.256	0.237
$j_{64}/j_{\lambda 4686}$	0.131	0.134	0.135	0.134
$j_{74}/j_{\lambda 4686}$	0.0678	0.0734	0.0779	0.0799
$j_{84}/j_{\lambda 4686}$	0.0452	0.0469	0.0506	0.0527
$j_{94}/j_{\lambda 4686}$	0.0280	0.0315	0.0345	0.0364
$j_{10,4}/j_{\lambda 4686}$	0.0198	0.0226	0.0249	0.0262
$j_{12,4}/j_{\lambda 4686}$	0.0106	0.0124	0.0139	0.0149
$j_{15,4}/j_{\lambda 4686}$	0.0050	0.0060	0.0069	0.0075
$j_{20,4}/j_{\lambda 4686}$	0.0020	0.0024	0.0029	0.0031
Pfund-line ($n \rightarrow 5$) intensities relative to $\lambda 4686$				
$j_{65}/j_{\lambda 4686}$	0.1081	0.0955	0.0856	0.0758
$j_{75}/j_{\lambda 4686}$	0.0547	0.0539	0.0513	0.0474
$j_{85}/j_{\lambda 4686}$	0.0320	0.0331	0.0327	0.0311
$j_{10,5}/j_{\lambda 4686}$	0.0144	0.0156	0.0160	0.0157
$j_{15,5}/j_{\lambda 4686}$	0.00320	0.00390	0.00430	0.00450
$j_{20,5}/j_{\lambda 4686}$	0.00120	0.00150	0.00170	0.00190

or

$$n_{nL} = \frac{(2L+1)}{n^2} n_n, \tag{4.18}$$

which is equivalent to $b_{nL} = b_n$, independent of L, where

$$n_n = \sum_{L=0}^{n-1} n_{nL}$$

is the total population in the levels with the same principal quantum number n. Since the cross sections $\sigma_{nL \to nL \pm 1}$ increase with increasing n, but the transition probabilities $A_{nL,n'L \pm 1}$ decrease, Equations (4.18) become increasingly good approximations with increasing n, and there is therefore (for any density and temperature) a level n_{cL} (for coupled angular momentum or "well L-mixed") above which they apply. For H at $T \approx 10,000$ K, this level is approximately $n_{cL} \approx 15$ at $n_p \approx 10^4$ cm^{-3}, $n_{cL} \approx 30$ at $n_p \approx 10^2$ cm^{-3} and $n_{cL} \approx 45$ at $n_p \approx 1$ cm^{-3}.

Exactly the same type of effect occurs in the He II spectrum, because it also has the property that all the levels nL with the same n are degenerate. The He II lines are emitted in the H$^+$, He^{++} zone of a nebula, so both protons and He^{++} ions (thermal α particles) can cause collisional, angular momentum-changing transitions in excited levels of He$^+$. The cross sections $\sigma_{nL \to nL \pm 1}$ actually are larger for the He^{++} ions than for the H$^+$ ions, and both of them must be taken into account in the He^{++} region. The principal quantum numbers above which (4.18) applies for He II at $T \approx 10,000$ K are approximately $n_{cL} \approx 22$ for $n_p \approx 10^4$ cm^{-3}, and $n_{cL} \approx 32$ for $n_p \approx 10^2$ cm^{-3}.

After the angular-momentum-changing collisions at fixed n, the next largest collisional transition rates occur for collisions in which n changes by ± 1, and of these the strongest are those for which L also changes by ± 1. For this type of transition, collisions with electrons are more effective than collisions with protons, and representative cross sections for thermal electrons at $T \approx 10,000$ K are of order $\sigma(nL \to n \pm \Delta n, L \pm 1) \approx 10^{-16}$ cm^2. The effects of these collisions can be incorporated into the equilibrium equations by a straightforward generalization of (4.16). Indeed, since the cross sections for collisions $\sigma(nL \to n \pm \Delta n, L \pm 1)$ decrease with increasing Δn (but not too rapidly), collisions with $\Delta n = 1, 2, 3, \ldots$ must all be included. The computational work required to set up and solve the equilibrium equations numerically becomes increasingly complicated and lengthy, but is straightforward in principle. It is clear that the collisions tend to couple levels with $\Delta L = \pm 1$ and small Δn, and that this coupling increases with increasing n_e (and n_p) and with increasing n. With collisions taken into account, the b_{nL} factors and the resulting emission coefficients are no longer independent of density.

Some calculated results for H I, including these collisional effects, are given in Table 4.4, which shows that the density dependence is rather small. Therefore this table, together with Table 4.2, which applies in the limit $n_e \to 0$, enables the H-line

emission coefficients to be evaluated over a wide range of densities and temperatures. Similarly, Table 4.5 shows calculated results for the He II recombination spectrum at finite densities and may be used in conjunction with Table 4.3, which applies in the same limit.

Exactly the same formalism can be applied to He I recombination lines, approximately treating the singlet and triplets as separate systems since all transition probabilities between them involving S, P, and D levels are quite small. The He I triplets always follow Case B, because downward radiative transitions to $1\,^1S$ essentially do not occur. For the singlets, Case B is ordinarily a better approximation than Case A for observed nebulae, though the optical depths are lower for all lines than for the corresponding lines of H by a factor of approximately the abundance ratio. An extra complication is that He I $1\,^1S$–$n\,^1P^o$ line photons can photoionize H^0, and thus may be destroyed before they are converted into lower-energy photons. Calculated (Case B) results for the strongest He I lines are summarized in Table 4.6, with $\lambda 4471$ ($2\,^3P^o$–$4\,^3D$) as the reference line. Note that only H itself and the ions of its isoelectronic sequence have energy levels with the same n but different L degenerate, so for He I, Table 4.6 lists the $j(n^{(2S+1)}L, n'^{(2S+1)}L)$, rather than $j(n, n')$, as for H. The radiative-transfer effects on the He I triplets, discussed in Section 4.6, and the collisional-excitation effects, discussed in Section 4.8, are not included in this table.

4.3 Optical Continuum Radiation

In addition to the line radiation emitted in the bound–bound transitions previously described, recombination processes also lead to the emission of rather weak continuum radiation in free–bound and free–free transitions. Because hydrogen is the most abundant element, the H I continuum, emitted in the recombination of protons with electrons, is the strongest, and the He II continuum may also be significant if He is mostly doubly ionized, but the He I continuum is always weaker. In the ordinary optical region the free–bound continua are stronger, but in the infrared and radio regions the free–free continuum dominates. In addition, there is a continuum resulting from the two-photon decay of the $2\,^2S$ level of H, which is populated by recombinations and subsequent downward cascading. In this section we will examine each of these sources of continuous radiation.

The H I free–bound continuum radiation at frequency ν results from recombinations of free electrons with velocity u to levels with principal quantum number $n \geq n_1$, and ionization potential X_n, where

$$h\nu = \frac{1}{2}u^2 + X_n \tag{4.19}$$

and

$$h\nu \geq X_{n_1} = \frac{h\nu_0}{n_1^2}, \tag{4.20}$$

Table 4.6

He I recombination lines (Case B)

				T			
	5,000 K		10,000 K			20,000 K	
n_e (cm^{-3})	10^2	10^4	10^2	10^4	10^6	10^2	10^4
$4\pi j_{\lambda 4471}/n_e n_{\mathrm{He^+}}$ (10^{-25} erg cm^3 s^{-1})	1.15	1.18	0.612	0.647	0.681	0.301	0.408
α_{4471}^{eff} (10^{-14} cm^3 s^{-1})	2.60	2.67	1.39	1.47	1.54	0.683	0.925
Triplet lines relative to $\lambda 4471$							
$j_{\lambda 5876}/j_{\lambda 4471}$	2.93	2.92	2.67	2.90	2.97	2.62	3.62
$j_{\lambda 4026}/j_{\lambda 4471}$	0.460	0.461	0.476	0.469	0.467	0.484	0.437
$j_{\lambda 7065}/j_{\lambda 4471}$	0.373	0.403	0.489	0.912	1.05	0.716	1.67
$j_{\lambda 10830}/j_{\lambda 4471}$	4.35	11.8	5.41	29.1	37.4	7.78	46.2
$j_{\lambda 3889}/j_{\lambda 4471}$	1.96	1.97	2.31	2.60	2.70	2.76	3.27
$j_{\lambda 3187}/j_{\lambda 4471}$	0.758	0.760	0.917	0.947	0.956	1.14	1.13
Singlet lines relative to $\lambda 4471$							
$j_{\lambda 6678}/j_{\lambda 4471}$	0.841	0.838	0.756	0.768	0.768	0.721	0.756
$j_{\lambda 4922}/j_{\lambda 4471}$	0.273	0.274	0.270	0.266	0.265	0.266	0.239
$j_{\lambda 5016}/j_{\lambda 4471}$	0.510	0.513	0.578	0.589	0.593	0.663	0.627
$j_{\lambda 3965}/j_{\lambda 4471}$	0.199	0.200	0.230	0.228	0.227	0.268	0.237

so its emission coefficient per unit frequency interval per unit solid angle per unit time per unit volume is therefore

$$j_\nu = \frac{1}{4\pi} n_p n_e \sum_{n=n_1}^{\infty} \sum_{L=0}^{n-1} u\sigma_{nL}(\mathrm{H^0}, u) f(u) \, h\nu \frac{du}{d\nu}. \quad (4.21)$$

The recombination cross sections $\sigma_{nL}(\mathrm{H^0}, u)$ can be calculated from the photoionization cross sections $a_\nu(\mathrm{H^0}, nL)$ by the Milne relation, as shown in Appendix 2.

The free–free (or bremsstrahlung) continuum emitted by free electrons accelerated in Coulomb collisions with positive ions (which are mostly H$^+$, He$^+$, or He^{++} in nebulae) of charge Z has an emission coefficient

$$j_\nu = \frac{1}{4\pi} n_+ n_e \frac{32 Z^2 e^4 h}{3m^2 c^3} \left(\frac{\pi h \nu_0}{3kT}\right)^{1/2} \exp(-h\nu/kT) \, g_{ff}(T, Z, \nu), \quad (4.22)$$

Table 4.7

H I continuous-emission coefficient (in 10^{-25} erg cm^3 s^{-1}) times frequency $\nu\gamma_\nu(\mathrm{H^0}, T)$

		T		
λ (μm)	5,000 K	10,000 K	15,000 K	20,000 K
10	0.310	0.262	0.238	0.223
3.0	1.03	0.772	0.673	0.618
1.0	1.87	1.72	1.57	1.46
0.8204+	1.23	1.54	1.55	1.52
0.8204−	8.70	4.18	2.99	2.45
0.700	5.71	3.69	2.90	2.49
0.5696	2.81	2.89	2.65	2.44
0.45	0.950	1.90	2.17	2.23
0.400	0.485	1.45	1.88	2.07
0.3646+	0.268	1.13	1.65	1.91
0.3646−	55.0	20.5	12.2	8.76
0.3122	21.3	13.8	9.82	7.72
0.260	3.39	6.17	6.21	5.79
0.150	0.0040	0.196	0.758	1.38
0.10	—	0.0025	0.0479	0.194

where $g_{ff}(T, Z, \nu)$ is a Gaunt factor. Thus the emission coefficient for the H I recombination continuum, including both bound–free and free–free contributions, may be written

$$j_\nu(\mathrm{H\,I}) = \frac{1}{4\pi} n_p n_e \gamma_\nu(\mathrm{H^0}, T). \quad (4.23)$$

Rather than tabulating and plotting this quantity itself, it is more convenient, especially for visualization, to use the quantity $\nu j_\nu(\mathrm{H\,I})$, which is proportional to the emission coefficient per unit logarithmic frequency interval $d\ln\nu = d\nu/\nu$. Numerical values for $\nu\gamma_\nu$, as calculated from Equations (4.21) and (4.22), are given in Table 4.7. Likewise, the contributions to the continuum-emission coefficient from He I and He II may be written

$$j_\nu(\mathrm{He\,I}) = \frac{1}{4\pi} n(\mathrm{He^+}) n_e \gamma_\nu(\mathrm{He^+}, T),$$

$$j_\nu(\mathrm{He\,II}) = \frac{1}{4\pi} n(\mathrm{He^{++}}) n_e \gamma_\nu(\mathrm{He^{++}}, T), \quad (4.24)$$

and numerical values of $\nu\gamma_\nu$ are listed in Tables 4.8 and 4.9. The calculation for He II is exactly analogous to that for H I, while for He I the only complication is that there is no L degeneracy and Equations (4.19), (4.20), and (4.21) must be appropriately

Table 4.8

He I continuous-emission coefficient (in 10^{-25} erg cm^3 s^{-1}) times frequency $\nu\gamma_\nu(\mathrm{He}^0, T)$

	T			
λ (μm)	5,000 K	10,000 K	15,000 K	20,000 K
10	0.310	0.262	0.238	0.223
3	1.02	0.77	0.67	0.62
1	1.90	1.72	1.57	1.46
0.8268+	1.27	1.55	1.55	1.51
0.8268−	2.02	1.81	1.70	1.61
0.8197+	2.08	1.84	1.71	1.62
0.8197−	5.61	3.09	2.39	2.06
0.7849+	4.99	2.97	2.37	2.06
0.7849−	7.91	4.01	2.93	2.43
0.7440+	6.86	3.83	2.89	2.44
0.7440−	7.06	3.90	2.93	2.47
0.6636+	5.01	3.48	2.82	2.46
0.6636−	5.54	3.67	2.92	2.53
0.5696	3.23	3.03	2.70	2.47
0.45	1.10	1.99	2.21	2.25
0.4	0.56	1.51	1.91	2.07
0.368+	0.33	1.20	1.69	1.93
0.368-	9.9	4.59	3.53	3.12
0.3433+	6.43	3.91	3.25	2.99
0.3433−	51.8	20.0	12.0	8.7
0.3122+	25.1	14.5	9.90	7.7
0.3122−	29.2	15.9	10.8	8.2
0.260+	5.54	7.51	6.87	6.12
0.260−	21.1	13.0	9.9	8.06
0.15	0.020	0.453	1.244	1.938
0.1	0.013	0.012	0.084	0.275

generalized. Figure 4.1 shows these calculated values $\nu\gamma_\nu$, and also shows the large discontinuities at the ionization potentials of the various excited levels. Note that for a typical He abundance of approximately 10 percent of that of H, if the He is mostly doubly ionized, then the He II contribution to the continuum is roughly comparable to that of H I, but if the He is mostly singly ionized, the He I contribution to the continuum is only about 10 percent of the H I contribution.

An additional important source of continuum emission in nebulae is the two-photon decay of the $2\,^2S$ level of H I, which is populated by direct recombinations and by cascades following recombinations to higher levels. The transition probability for this two-photon decay is $A_{2\,^2S,1\,^2S} = 8.23$ s^{-1}, and the sum of the energies of the two photons is $h\nu' + h\nu'' = h\nu_{12} = h\nu\,(\mathrm{L}\alpha) = (3/4)h\nu_0$. The probability distribution

Table 4.9

He II continuous-emission coefficient times frequency (in 10^{-25} erg cm^3 s^{-1}) $\nu\gamma_\nu(\mathrm{He}^+, T)$

	T			
λ (μm)	5,000 K	10,000 K	15,000 K	20,000 K
10	1.00	0.897	0.826	0.777
3	2.91	2.45	2.23	2.09
1	11.5	7.96	6.61	5.89
0.820+	7.64	7.16	6.57	6.14
0.820−	23.0	12.6	9.53	8.07
0.700	15.0	11.0	9.20	8.16
0.5694+	7.30	8.57	8.33	7.96
0.5694−	45.3	22.0	15.6	12.7
0.450	15.3	14.5	12.9	11.7
0.400	7.82	11.0	11.2	10.8
0.3644+	4.34	8.62	9.76	9.99
0.3644−	119.4	49.3	31.9	24.4
0.312	37.8	30.2	24.4	20.8
0.260	7.34	14.7	16.1	15.9
0.150	3.98	18.7	25.4	27.2
0.100	0.174	0.395	1.77	3.99

of the emitted photons is therefore symmetric around the frequency $(1/2)\nu_{12} = 1.23 \times 10^{15}$ s^{-1}, corresponding to $\lambda = 2431$ Å. The emission coefficient in this two-photon continuum may be written

$$j_\nu(2q) = \frac{1}{4\pi}n_2\,{}^2S A_{2\,^2S,1\,^2S} 2h\nu P(y), \tag{4.25}$$

where $P(y)dy$ is the normalized probability per decay that one photon is emitted in the range of frequencies $y\,\nu_{12}$ to $(y + dy)\nu_{12}$.

To express this two-photon continuum-emission coefficient in terms of the proton and electron density, it is necessary to calculate the equilibrium population of $n(2\,^2S)$ in terms of these quantities. In sufficiently low-density nebulae, two-photon decay is the only mechanism that depopulates $2\,^2S$, and the equilibrium is given by

$$n_p n_e \alpha_{2^2S}^{eff}(\mathrm{H}^0, T) = n_2\,{}^2S A_{2\,^2S,1\,^2S} \tag{4.26}$$

where $\alpha_{2^2S}^{eff}$ is the effective recombination coefficient for populating $2\,^2S$ by direct recombinations and by recombinations to higher levels followed by cascades to $2\,^2S$. However, at finite densities, angular-momentum-changing collisions of protons and electrons with H atoms in the $2\,^2S$ level shift the atoms to $2\,^2P^o$ and thus remove them
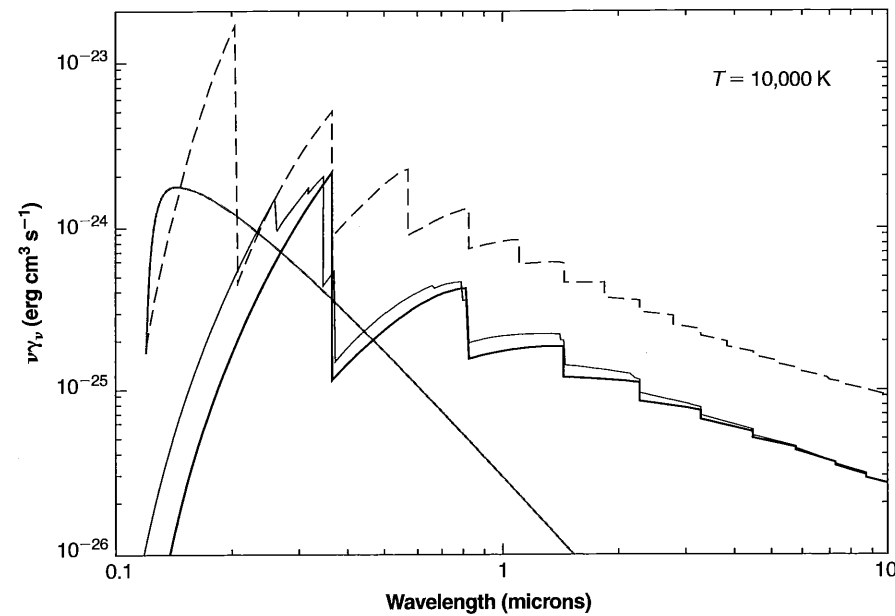
Figure 4.1
Frequency variation of continuous-emission coefficient $\gamma_\nu(H^0$, solid line), γ_ν (He^0, thin solid line), γ_ν (He$^+$, dashed line), and γ_ν ($2h\nu$, smooth solid line) in the low-density limit $n_e \to 0$, all at $T = 10,000$ K.

from $2\,^2S$. The protons are more effective than electrons, whose effects, however, are not completely negligible, as can be seen from the values of the collisional transition rates per $2\,^2S$ atom, in Table 4.10. With these collisional processes taken into account, the equilibrium population in $2\,^2S$ is given by

$$n_p n_e \alpha_{2\,^2S}^{eff}(H^0, T) =$$
$$n_{2\,^2S}\left(A_{2\,^2S,1\,^2S} + n_p q_{2\,^2S,2\,^2P^o}^p + n_e q_{2\,^2S,2\,^2P^o}^e\right). \tag{4.27}$$

From Table 4.10, it can be seen that collisional deexcitation of $2\,^2S$ via $2\,^2P^o$ is more important than two-photon decay for $n_p \geq 10^4$ cm^{-3}; so at densities approaching this value, Equation (4.27) must be used instead of Equation (4.26). Thus combining Equations (4.25) and (4.27), we can write the emission coefficient as

$$j_\nu(2q) = \frac{1}{4\pi} n_p n_e \gamma_\nu(2q) \tag{4.28}$$

Table 4.10
Collisional transition rate coefficients (in cm^3 s^{-1}) for H I $2\,^2S$, $2\,^2P^o$

	T	
	10,000 K	20,000 K
	Protons	
$q_{2\,^2S,2\,^2P^o_{1/2}}^p$	2.51×10^{-4}	2.08×10^{-4}
$q_{2\,^2S,2\,^2P^o_{3/2}}^p$	2.23×10^{-4}	2.19×10^{-4}
	Electrons	
$q_{2\,^2S,2\,^2P^o_{1/2}}^e$	0.22×10^{-4}	0.17×10^{-4}
$q_{2\,^2S,2\,^2P^o_{3/2}}^e$	0.35×10^{-4}	0.27×10^{-4}
	Total	
$q_{2\,^2S,2\,^2P^o}$	5.31×10^{-4}	4.71×10^{-4}

Table 4.11
Effective recombination coefficient (in cm^3 s^{-1}) to H ($2\,^2S$)

T (K)	$\alpha_{2\,^2S}^{eff}$
5,000	1.38×10^{-13}
10,000	0.838×10^{-13}
15,000	0.625×10^{-13}
20,000	0.506×10^{-13}

where

$$\gamma_\nu(2q) = \frac{\alpha_{2\,^2S}^{eff}(H^0, T) g_\nu}{1 + \left[\dfrac{n_p q_{2\,^2S,2\,^2P}^p + n_e q_{2\,^2S,2\,^2P}^e}{A_{2\,^2S,1\,^2S}}\right]} \tag{4.29}$$

The quantity $\alpha_{2\,^2S}^{eff}$ is tabulated in Table 4.11 and νg_ν is tabulated in Table 4.12. The two-photon continuum is also plotted in Figure 4.1 for $T = 10,000$ K and in the low-density limit $n_p \approx n_e \ll 10^4$ cm^{-3}. It can be seen that this continuum is quite significant in comparison with the H I continua, particularly just above the Balmer limit at $\lambda 3646$ Å. Note that although the two-photon continuum is symmetric about $\nu_{12}/2$ if expressed in photons per unit frequency interval, it is not symmetric about $\lambda 2431$ if expressed per

Table 4.12

Spectral distribution of H I two-photon emission (in 10^{-12} erg) νg_ν

λ (Å)	$\nu(10^{14}$ Hz)	νg_ν
∞	0.0	0.0
24,313	1.23	0.0373
12,157	2.47	0.242
8104	3.70	0.679
6078	4.93	1.37
4863	6.17	2.33
4052	7.40	3.55
3473	8.64	5.01
3039	9.87	6.69
2701	11.10	8.59
2431	12.34	10.6

unit wavelength interval, nor is either symmetric if expressed in energy units rather than photons. From Equation (4.25), if $\nu > \nu_{12}/2$,

$$g_\nu = \frac{\nu}{\nu'} g_{\nu'},$$

where $\nu' = \nu_{12} - \nu$.

4.4 Radio-Frequency Continuum and Line Radiation

The line and continuous spectra described in Sections 4.2 and 4.3 extend to arbitrarily low frequency, and in fact give rise to observable features in the radio-frequency spectrum region. Though this "thermal" radio-frequency radiation is a natural extension of the optical line and continuous spectra, it is somewhat different, in detail, because in the radio-frequency region $h\nu \ll kT$, and stimulated emission, which is proportional to $\exp(-h\nu/kT)$, is therefore much more important in that region than in the ordinary optical region. We will examine the continuous spectrum first, and then the recombination-line spectrum.

In the radio-frequency region, the continuum is due to free–free emission, and the emission coefficient is given by the same Equation (4.22) that applies in the optical region. However, in the radio-frequency region, the Gaunt factor $g_{ff}(T, Z, \nu) \not\approx 1$, as in the optical region, but rather

$$g_{ff}(T, Z, \nu) = \frac{\sqrt{3}}{\pi} \left[\ln \left(\frac{8k^3 T^3}{\pi^2 Z^2 e^4 m \nu^2} \right)^{1/2} - \frac{5\gamma}{2} \right], \tag{4.30}$$

where $\gamma = 0.577$ is Euler's constant. Numerically, this is approximately

$$g_{ff}(T, Z, \nu) = \frac{\sqrt{3}}{\pi} \left(\ln \frac{T^{3/2}}{Z\nu} + 17.7 \right),$$

with T in K and ν in Hz, and thus at $T \approx 10,000$ K, $\nu \approx 10^3$ MHz, $g_{ff} \approx 10$.

The free–free effective absorption coefficient can then be found from Kirchhoff's law, and is

$$\kappa_\nu = n_+ n_e \frac{16\pi^2 Z^2 e^6}{(6\pi mkT)^{3/2} \nu^2 c} g_{ff} \tag{4.31}$$

per unit length. Note that this effective absorption coefficient is the difference between the true absorption coefficient and the stimulated emission coefficient, since the stimulated emission of a photon is exactly equivalent to a negative absorption process; in the radio-frequency region ($h\nu \ll kT$) the stimulated emissions very nearly balance the true absorptions and the correction for stimulated emission $[1 - \exp(h\nu/kT)] \approx h\nu/kT \ll 1$.

Substituting numerical values and fitting powers to the weak temperature and frequency dependence of g_{ff},

$$
\begin{aligned}
\tau_\nu &= \int \kappa_\nu \, ds \\
&= 8.24 \times 10^{-2} T^{-1.35} \nu^{-2.1} \int n_+ n_e \, ds \\
&= 8.24 \times 10^{-2} T^{-1.35} \nu^{-2.1} E_c.
\end{aligned}
\tag{4.32}
$$

In this formula T is measured in K, ν in GHz, and E_c, the so-called continuum emission measure, in cm^{-6} pc. It can be seen from Equations (4.31) or (4.32) that at sufficiently low frequency all nebulae become optically thick; for example, an H II region with $n_e \approx n_p \approx 10^2$ cm^{-3} and a diameter 10 pc has $\tau_\nu \approx 1$ at $\nu \approx 200$ MHz, and a planetary nebula with $n_e \approx 3 \times 10^3$ cm^{-3} and a diameter of 0.1 pc has $\tau_\nu \approx 1$ at $\nu \approx 600$ MHz. Thus, in fact, many nebulae are optically thick at observable low frequencies and optically thin at observable high frequencies. The equation of radiative transfer,

$$\frac{dI_\nu}{ds} = -\kappa_\nu I_\nu + j_\nu \tag{4.33}$$

or

$$\frac{dI_\nu}{d\tau_\nu} = -I_\nu + \frac{j_\nu}{\kappa_\nu} = -I_\nu + B_\nu(T), \tag{4.34}$$

has the solution for no incident radiation

$$I_\nu = \int_0^{\tau_\nu} B_\nu(T) \exp(-\tau_\nu) d\tau_\nu. \tag{4.35}$$

In the radio-frequency region,

$$B_\nu(T) = \frac{2h\nu^3}{c^2} \frac{1}{\exp(h\nu/kT) - 1} \approx \frac{2\nu^2 kT}{c^2} \tag{4.36}$$

is proportional to T, so it is conventional in radio astronomy to measure intensity in terms of brightness temperature, defined by $T_{bn} = c^2 I_\nu / 2\nu^2 k$. Hence (4.35) can be rewritten

$$T_{b\nu} = \int_0^\tau T \exp(-\tau_\nu) \, d\tau_\nu, \tag{4.37}$$

and for an isothermal nebula, this becomes

$$T_{b\nu} = T[1 - \exp(\tau_\nu)] \begin{bmatrix} \to T\tau_\nu \ as \ \tau_\nu \to 0 \\ \to T \ as \ \tau_\nu \to \infty \end{bmatrix}.$$

Thus the radio-frequency continuum has a spectrum in which $T_{b\nu}$ varies approximately as ν^{-2} at high frequency and is independent of ν at low frequency.

The H I recombination lines of very high n also fall in the radio-frequency spectral region and have been observed in many gaseous nebulae. Some specific examples of observed lines are H 109α (the transition with $\Delta n = 1$ from $n = 110$ to $n = 109$) at $\nu = 5008.89$ MHz, $\lambda = 5.99$ cm, H 137β (the transition with $\Delta n = 2$ from $n = 139$ to $n = 137$) at $\nu = 5005.0$ MHz, $\lambda = 6.00$ cm, and so on. The emission coefficients in these radio recombination lines may be calculated from equations similar to those described in Section 4.2 for the shorter wavelength optical recombination lines. For all lines observed in the radio-frequency region, $n > n_{cL}$ defined there, so that at a fixed n, $n_{nL} \propto (2L + 1)$, and only the populations n_n need be considered. One additional process, in addition to those described in Section 4.2, must also be taken into account, namely collisional ionization of levels with large n and its inverse process, three-body recombination,

$$H^0(n) + e \Leftrightarrow H^+ + e + e.$$
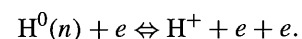
The rate of collisional ionization per unit volume per unit time from level n may be written

$$n_n n_e \overline{u\sigma_{ionization}(n)} = n_n n_e q_{n,i}(T), \tag{4.38}$$

and the rate of three-body recombination per unit time per unit volume may be written $n_p n_e^2 \phi_n(T)$; so, from the principle of detailed balancing,

$$\phi_n(T) = n^2 \left(\frac{h^2}{2\pi mkT}\right)^{3/2} \exp(X_n/kT) q_{n,i}(T). \tag{4.39}$$

Thus the equilibrium equation that is analogous to Equation (4.16) becomes, at high n,

$$
\begin{aligned}
n_p n_e &\left[\alpha_n(T) + n_e \phi_n(T)\right] + \sum_{n'>n}^{\infty} n_{n'} A_{n',n} + \sum_{n'=n_0}^{\infty} n_{n'} n_e q_{n',n} \\
&= n_n \left[\sum_{n'=n_0}^{n-1} A_{n,n'} + \sum_{n'=n_0}^{\infty} n_e q_{n,n'}(T) + n_e q_{n,i}(T)\right],
\end{aligned}
\tag{4.40}
$$

where

$$A_{n,n'} = \frac{1}{n^2} \sum_{L,L'} (2L + 1) A_{nL,n'L'} \tag{4.41}$$

is the mean transition probability averaged over all the L levels of the upper principal quantum number. These equations can be expressed in terms of b_n instead of n_n, and the solutions can be found numerically by standard matrix-inversion techniques. Note that since the coefficients b_n have been defined with respect to thermodynamic equilibrium at the local T, n_e, and n_p, the coefficient b for the free electrons is identically unity, and therefore $b_n \to 1$ as $n \to \infty$. Some calculated values of b_n for $T = 10{,}000$ K and various n_e are plotted in Figure 4.2, which shows that the increasing importance of collisional transitions as n_e increases makes $b_n \approx 1$ at lower and lower n.

To calculate the emission in a specific recombination line, it is again necessary to solve the equation of transfer, taking account of the effects of stimulated emission. In this case, for an n, Δn line between the upper level $m = n + \Delta n$ and the lower level n, if $k_{\nu l}$ is the true line-absorption coefficient, then the line-absorption coefficient, corrected for stimulated emission, to be used in the equation of transfer is

$$k_{\nu l} = k_{\nu l} \left(1 - \frac{b_m}{b_n} \exp(-h\nu/kT)\right), \tag{4.42}$$

since it is the net difference between the rates of upward absorption processes and of downward-induced emissions. If we expand (4.42) in a power series, it becomes

$$k_{\nu L} = k_{\nu l} \left(\frac{b_m}{b_n} \frac{h\nu}{kT} - \frac{d\ln(b_n)}{dn} \Delta n\right). \tag{4.43}$$

Since $b_m/b_n \approx 1$ and $h\nu \ll kT$, the line-absorption coefficient can become negative, implying positive maser action, if $(d \ln b_n)/dn$ is sufficiently large. Calculated values of this derivative are therefore also shown in Figure 4.2. Since, for typical observed lines $h\nu/kT \approx 10^{-5}$, it can be seen from this figure that the maser effect is in fact often quite important. We will again use these concepts and expressions to calculate the strengths of the radio-frequency recombination lines in Chapter 5.
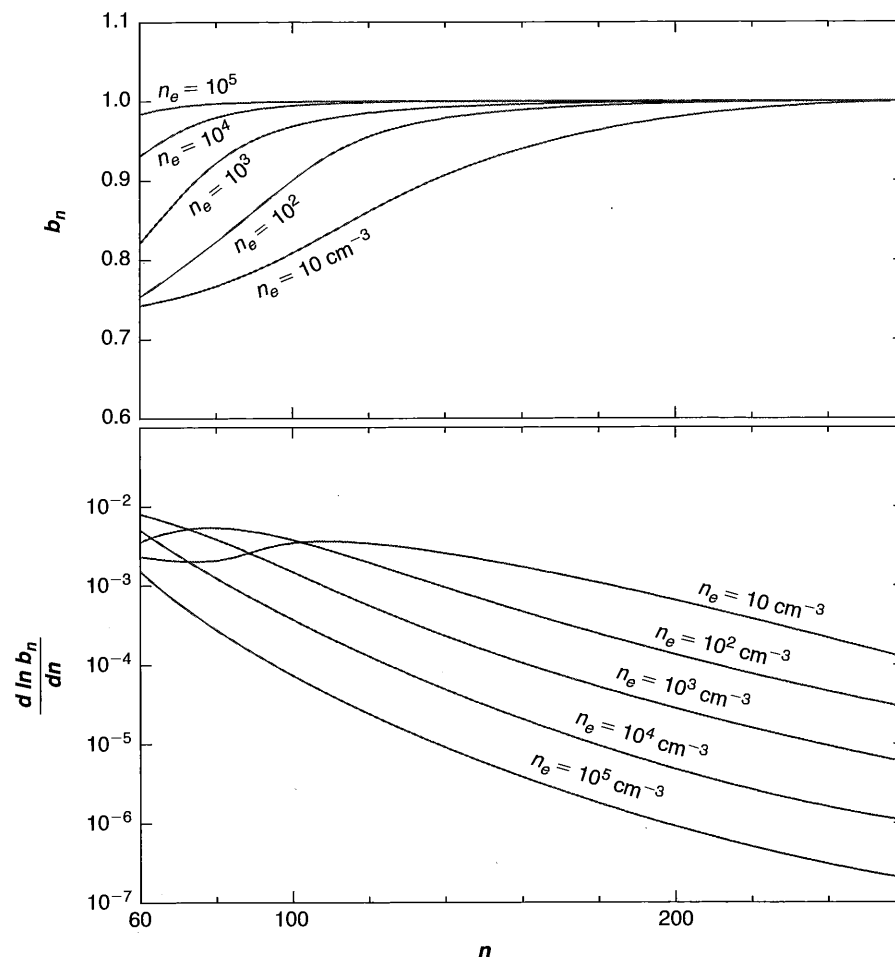
Figure 4.2

Dependence of b_n and $d \ln b_n/dn$ on n at various densities, all at $T = 10,000$ K.

4.5 Radiative Transfer Effects in H I

For most of the emission lines observed in nebulae there is no radiative-transfer problem; in most lines the nebulae are optically thin, and any line photon emitted simply escapes. However, in some lines, especially the resonance lines of abundant atoms, the optical depths are appreciable, and scattering and absorption must be taken into account in calculating the expected line strengths. Two extreme assumptions, Case A, a nebula with vanishing optical thickness in all the H I Lyman lines, and Case B, a nebula with large optical depths in all the Lyman lines, have already been discussed in

Section 4.2; and although these two cases do not require a detailed radiative-transfer solution, in the intermediate cases a more sophisticated treatment is necessary. Other radiative-transfer problems arise in connection with the He I triplets, the conversion of He II Lα and H I Lβ into observable O III or O I line radiation, respectively, by the Bowen resonance-fluorescence processes, and fluorescence excitation of other lines by stellar continuum radiation. In this section some general concepts about the escape of line photons from nebulae will be discussed in the context of the H I Lyman and Balmer lines, and then in succeeding sections these same concepts will be applied to the other problems mentioned.

In a static nebula the only line-broadening mechanisms are thermal Doppler broadening and radiative damping, and in the cores of the lines, where radiative damping can be neglected, the line-absorption coefficient has the Doppler form

$$\kappa_{vl} = k_{0l} \exp\left[- \left(\Delta v/\Delta v_D\right)^2 \right] = k_{0l} \exp(-x^2) \quad [\text{cm}^2], \tag{4.44}$$

where

$$k_{0l} = \frac{\lambda^2}{8\pi^{3/2}} \frac{\omega_j}{\omega_i} \frac{A_{j,i}}{\Delta v_D} = \frac{\sqrt{\pi}e^2 f_{ij}}{mc\Delta v_D} \quad [\text{cm}^2] \tag{4.45}$$

is the line-absorption cross section per atom at the center of the line,

$$\Delta v_D = \sqrt{\frac{2kT}{m_H c^2}} v_0 \quad [\text{Hz}]$$

is the thermal Doppler width (Hz), and f_{ij} is the absorption oscillator strength between the lower and upper level i, j. The full-width at half-maximum (FWHM) of the line is $2\sqrt{\ln 2}$ times larger than Δv_D. Small-scale micro-turbulence can be taken into account as a further source of broadening of the line-absorption coefficient by adding the thermal and turbulent velocity terms in quadrature, $\Delta v_D^2 = \Delta v_{thermal}^2 + \Delta v_{turbulent}^2$. Larger scale turbulence and expansion of the nebula can be treated by considering the frequency shift between the emitting and absorbing volumes.

In a static nebula, a photon emitted at a particular point in a particular direction and with a normalized frequency x from the center of the line has a probability $\exp(-\tau_x)$ of escaping from the nebula without further scattering and absorption. Here τ_x is the optical depth from the point to the edge of the nebula in this direction and at this frequency. Averaging over all directions gives the mean escape probability from this point and at this frequency, and further averaging over the frequency profile of the emission coefficient gives the mean escape probability from the point.

For all the forbidden lines and for most of the other lines, the optical depths are so small in every direction, even at the center of the line, that the mean escape probabilities from all points are essentially unity. However, for lines of larger optical depth we must examine the probability of escape quantitatively.

Consider an idealized spherical homogeneous nebula, with optical radius in the center of line τ_{0l}. So long as $\tau_{0l} < 10^4$, only the Doppler core of the line-absorption cross section need be considered. The photons are emitted with the same Doppler profile, and the mean probability of escape must therefore be averaged over this profile. If, at a particular normalized frequency x, the optical radius of the nebula is τ_x, the mean probability of escape averaged over all directions and volumes is

$$p\left(\tau_\chi\right) = \frac{3}{4\tau_x}\left[1 - \frac{1}{2\tau_x^2} + \left(\frac{1}{\tau_x} + \frac{1}{2\tau_x^2}\right)\exp(-2\tau_x)\right]. \tag{4.46}$$

When we average over the Doppler profile, the mean escape probability for a photon emitted in the line is

$$\varepsilon\left(\tau_{0l}\right) = \frac{1}{\sqrt{\pi}}\int_{-\infty}^{\infty} p\left(\tau_x\right)\exp(-x^2)dx \tag{4.47}$$

where τ_{0l} is the optical radius in the center of the line. This integral must be evaluated numerically, but for optical radii ($\tau_{0l} \leq 50$) that are not too large, the results can be fitted fairly accurately with $\varepsilon(\tau_{0l}) = 1.72/(\tau_{0l} + 1.72)$.

If we consider a Lyman line Ln, photons emitted in this line that do not escape from the nebula are absorbed by another hydrogen atom, and each absorption process represents an excitation of the $n\,^2P^o$ level of H I. This excited level very quickly undergoes a radiative decay, and the result is either resonance scattering or resonance fluorescence excitation of another H I line. If the photon emitted from the n^2P level decays in a $1\,^2S$–$n\,^2P^o$ transition, the process is resonance scattering of an Ln photon. If it is emitted in the $2\,^2S$–$n\,^2P^o$ transition, the process is conversion of Ln into Hn plus excitation of $2\,^2S$, leading to emission of two photons in the continuum. If it is emitted in the $3\,^2S$–$n\,^2P^o$ transition, the process is conversion of Ln into Pn plus excitation of $3\,^2S$, leading to emission of Hα plus Lα, and so on. The probabilities of each of these processes may be found directly from the probability matrices $C_{nL,n'L'}$ and $P_{nL,n'L'}$, defined in Section 4.2. If we define $P_n(\text{L}m)$ and $P_n(\text{H}m)$ as the probabilities that absorption of an Ln photon results in emission of an Lm photon and of an Hm photon, respectively, then

$$P_n(\text{L}m) = C_{n1,m1}P_{m1,10} \tag{4.48}$$

and

$$P_n(\text{H}m) = C_{n1,m0}P_{m0,21} + C_{n1,m1}P_{m1,20} + C_{n1,m2}P_{m2,21}. \tag{4.49}$$

We can now use these probabilities to calculate the emergent Lyman-line spectrum emitted from a model nebula. It is easiest to work in terms of numbers of photons emitted. If we write R_n for the total number of Ln photons generated in the nebula per unit time by recombination and subsequent cascading, and A_n as the total number of Ln photons absorbed in the nebula per unit time, then J_n, the total number of

Ln photons emitted in the nebula per unit time, is the sum of the contributions from recombination and from resonance fluorescence plus scattering:

$$J_n = R_n + \sum_{m=n}^{\infty} A_m P_m(\text{L}n). \tag{4.50}$$

Since each Ln photon emitted has a probability ε_n of escaping, the total number of Ln photons escaping the nebula per unit time is

$$E_n = \varepsilon_n J_n = \varepsilon_n\left[R_n + \sum_{m=n}^{\infty} A_m P_m(\text{L}n)\right]. \tag{4.51}$$

Finally, in a steady state the number of Ln photons emitted per unit time is equal to the sum of the numbers absorbed and escaping per unit time,

$$J_n = A_n + E_n = A_n + \varepsilon_n J_n. \tag{4.52}$$

Thus, eliminating J_n between (4.51) and (4.52),

$$A_n = (1 - \varepsilon_n)\left[R_n + \sum_{m=n}^{\infty} A_m P_m(\text{L}n)\right], \tag{4.53}$$

and since the R_n and $P_m(\text{L}n)$ are known from the recombination theory and the ε_n are known from the radiative-transfer theory, Equation (4.53) can be solved for the A_n by a systematic procedure, working downward from the highest n at which ε_n differs appreciably from unity. Then from these values of R_n, the E_n may be calculated from (4.51), giving the emergent Lyman-line spectrum.

Next we will investigate the Balmer-line spectrum, which requires further analysis. Let us write S_n for the number of Hn photons generated in the nebula per unit time by recombination and subsequent cascading. Suppose that there is no absorption of these Balmer-line photons, so that K_n, the total number of Hn photons emitted in the nebula per unit time, is the sum of contributions from recombination and from resonance fluorescence due to Lyman-line photons,

$$K_n = S_n + \sum_{m=n}^{\infty} A_m P_m(\text{H}n).$$

Then, since the S_n and $P_m(\text{H}n)$ are known from the recombination theory and the A_m are known from the previous Lyman-line solution, the K_n can be calculated immediately to obtain the emergent Balmer-line spectrum. Note that R_n, S_n, J_n, K_n, and A_n are proportional to the total number of photons; the equations are linear in these quantities; and the entire calculation can therefore be normalized to any S_n, for instance, to S_4, the number of Hβ photons that would be emitted if there were no absorption effects. The results, in the form of calculated ratios of Hα/Hβ and Hβ/Hγ intensities, are shown in Figure 4.3 as a function of $\tau_{0l}(\text{L}\alpha)$, the optical radius of
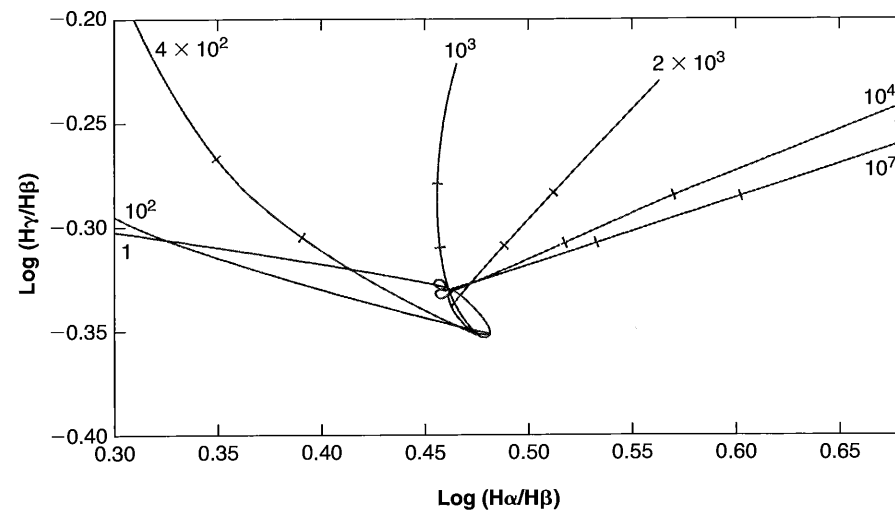
Figure 4.3

Radiative transfer effects caused by finite optical depths in Lyman and Balmer lines. Ratios of total emitted fluxes $H\alpha/H\beta$ are shown for homogeneous static isothermal model nebulae at $T = 10{,}000$ K. Each line connects a series of models with the $\tau_{0l}(L\alpha)$, given at the end of the line; along it $\tau_{0l}(H\alpha) = 5$ and 10 at the two points along each line indicated by bars for $\tau_{0l}(L\alpha) \geq 400$.

the nebula at the center of $L\alpha$; and the transition from Case A ($\tau_{0l} \to 0$) to Case B ($\tau_{0l} \to \infty$) can be seen clearly.

Although in most nebulae, the optical depths in the Balmer lines are small, there could be situations in which the density $n(H^0, 2\,^2S)$ is sufficiently high that some self-absorption does occur in these lines. The optical depths in the Balmer lines can again be calculated from Equation (4.45), and since they are proportional to n (H^0, $2\,^2S$), the radiative-transfer problem is now a function of two variables, $\tau_{0l}(L\alpha)$, giving the optical radius in the Lyman lines, and another, say, $\tau_{0l}(H\alpha)$, giving the optical radius in the Balmer lines. Although the equations are much more complicated, since now Balmer-line photons may be scattered or converted into Lyman-line photons and vice versa, there is no new effect in principle, and the same general type of formulation developed previously for the Lyman-line absorption can still be used. We will not examine the details here, but will simply discuss physically the calculated results shown in Figure 4.3. For $\tau_{0l}(H\alpha) = 0$, the first effect of increasing $\tau_{0l}(L\alpha)$ is that $L\beta$ is converted into $H\alpha$ plus the two-photon continuum. This increases the $H\alpha/H\beta$ ratio of the escaping photons, corresponding to a move of the representative point to the right in Figure 4.3. However, for slightly larger $\tau_{0l}(L\alpha)$, $L\gamma$ photons are also converted into $P\alpha$, $H\alpha$, $H\beta$, $L\alpha$, and two-photon continuum photons, and since the main effect is to increase the strength of $H\beta$, this corresponds to a move downward and to the left in Figure 4.3. For still larger $\tau_{0l}(L\alpha)$, as still higher Ln photons are

converted, $H\gamma$ is also strengthened, and the calculation, which takes into account all of these effects, shows that the representative point describes the small loop of Figure 4.3 as the conditions change from Case A to Case B. For large $\tau_{0l}(L\alpha)$, the effect of increasing $\tau_{0l}(H\alpha)$ is that, although $H\alpha$ is merely scattered (because any $L\beta$ photons it forms are quickly absorbed and converted back to $H\alpha$), $H\beta$ is absorbed and converted to $H\alpha$ plus $P\alpha$. This increases $H\alpha/H\beta$ and decreases $H\beta/H\gamma$, as shown quantitatively in Figure 4.3.

4.6 Radiative Transfer Effects in He I

The recombination radiation of He I singlets is very similar to that of H I, and Case B is a good approximation for the He I Lyman lines. However, the recombination radiation of the He I triplets is modified by the fact that the $He^0\, 2\,^3S$ term is considerably more metastable than $H^0\, 2\,^2S$, and as a result self-absorption effects are quite important (as is collisional excitation from $2\,^3S$, to be discussed later). As the energy-level diagram of Figure 4.4 shows, $2\,^3S$ is the lowest triplet term in He, and recaptures to triplets tend to cascade down to it. Depopulation occurs only by photoionization, especially by H I $L\alpha$, by collisional transitions to $2\,^1S$ and $2\,^1P^o$, or by the strongly forbidden $2\,^3S$–$1\,^1S$ radiative transition, as discussed in Section 2.4. As a result $n(2\,^3S)$ is large, which in turn makes the optical depths in the lower $2\,^3S$–$n\,^3P^o$ lines significant. Figure 4.4 shows that $\lambda10830\, 2\,^3S$–2^3P^o photons are simply scattered, but that absorption of $\lambda3889\, 2\,^3S$–3^3P^o photons can lead to their conversion to $\lambda4.3\ \mu m\, 3\,^3S$–$3^3P^o$, plus $2\,^3P$–$3\,^3S\lambda7065$, plus $2\,^3S$–$2^3P^o\lambda10830$. The probability of this conversion is

$$\frac{A_{3\,^3S,3\,^3P^o}}{A_{3\,^3S,3\,^3P^o} + A_{2\,^3S,3\,^3P^o}} \approx 0.10$$

per absorption. At larger $\tau_{0l}(\lambda10830)$, still higher members of the $2\,^3S$–$n\,^3P^o$ series are converted into longer wavelength photons.

The radiative-transfer problem is very similar to that for the Lyman lines discussed in Section 4.5, and may be handled by the same kind of formalism. Calculated ratios of the intensities of $\lambda3889$ (which is weakened by self-absorption) and of $\lambda7065$ (which is strengthened by resonance fluorescence) relative to the intensity of $\lambda4471$ $2\,^3P^o$–$4\,^3D$ (which is only slightly affected by absorption) are shown for spherically symmetric homogeneous model nebulae in Figure 4.5.

The thermal Doppler widths of He I lines are smaller than those of H I lines, because of the larger mass of He, and therefore whatever turbulent or expansion velocity there may be in a nebula is relatively more important in broadening the He I lines. The simplest example to consider is a model spherical nebula expanding with a linear velocity of expansion,

$$U_{\exp}(r) = \omega\, r;\ 0 \leq r \leq R; \tag{4.54}$$
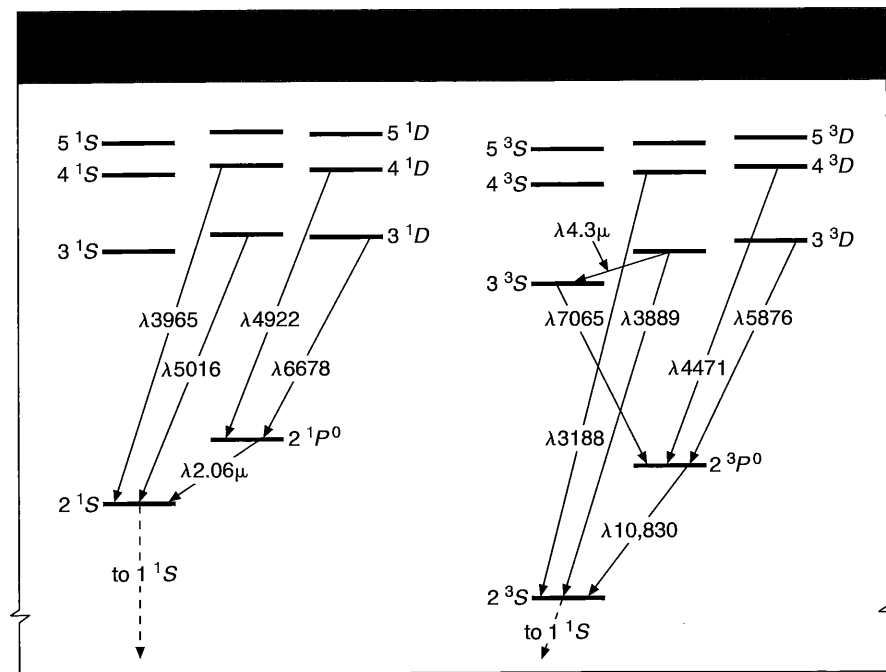
Figure 4.4

Partial energy-level diagram of He I, showing strongest optical lines observed in nebulae. Note that $1\,^2S$ has been omitted, and terms with $n \geq 6$ or $L \geq 3$ have been omitted for the sake of space and clarity.

for then, between any two points r_1 and r_2 in the nebula, the relative radial velocity is

$$u(r_1, r_2) = \omega\, s, \tag{4.55}$$

where s is the distance between the points and ω is the constant velocity gradient. Thus photons emitted at r_1 will have a line profile centered about the line frequency ν_L in the reference system in which r_1 is at rest. However, they will encounter at r_2 material absorbing with a profile centered on the frequency

$$\nu'(r_1, r_2) = \nu_L \left(1 + \frac{\omega\, s}{c}\right), \tag{4.56}$$

and the optical depth in a particular direction to the boundary of the nebula for a photon emitted at r_1 with frequency ν may be written

$$\tau_\nu(r_1) = \int_0^{r_2=R} n(2\,^3S)k_{0l}\exp\left\{-\left[\frac{\nu - \nu'(r_1, r_2)}{\Delta\nu_D}\right]^2\right\}ds. \tag{4.57}$$
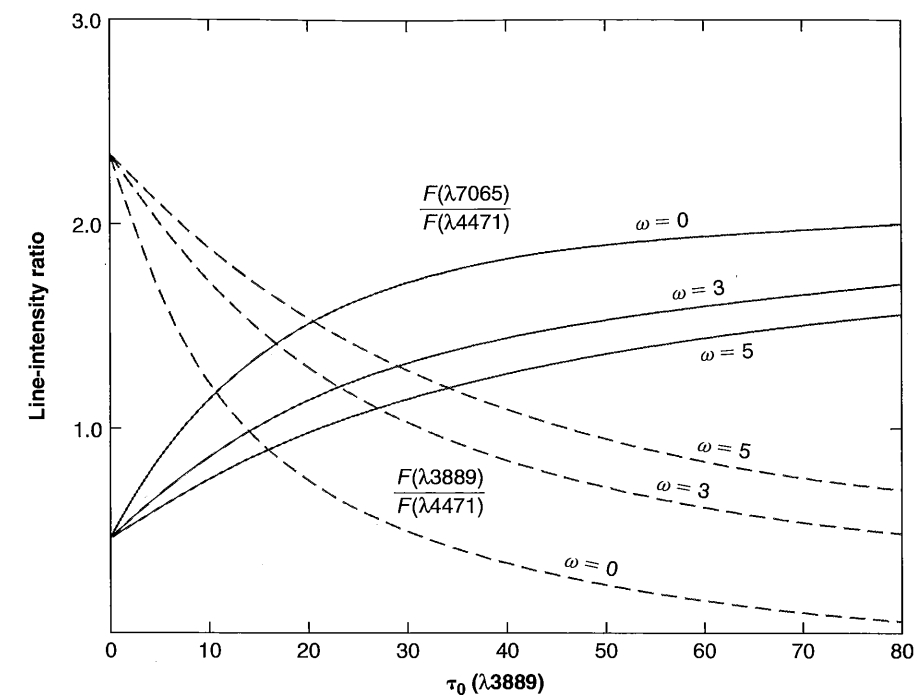
Figure 4.5

Radiative transfer effects due to finite optical depths in He I $\lambda 3889$ $2\,^3S$–$3\,^3P^o$. Ratios of emergent fluxes of $\lambda 7065$ and $\lambda 3889$ to the flux in $\lambda 4471$ are as a function of optical radius $\tau_0(\lambda 3889)$ of homogeneous static ($\omega = 0$) and expanding ($\omega \neq 0$) isothermal nebulae at $T = 10{,}000$ K.

It can be seen that increasing velocity of expansion tends, for a fixed density $n(2\,^3S)$, to decrease the optical depth to the boundary of the nebula and thus to decrease the self-absorption effects. This effect can be seen in Figure 4.5, where some calculated results are shown for various ratios of the expansion velocity $u_{exp}(R) = \omega R$ to the thermal velocity $u_{th} = (2kT/m_{\mathrm{He}})^{1/2}$, as functions of $\tau_{0l}(\lambda 3889) = n(2\,^3S)\kappa_{0l}(\lambda 3889)R$, the optical radius at the center of the line for zero expansion velocity. Note that the calculated intensity ratios for large u_{exp}/u_{th} and large τ_0 are quite similar to those for smaller u_{exp}/u_{th} and smaller τ_0.

4.7 The Bowen Resonance-Fluorescence Mechanisms for O III and O I

There is an accidental coincidence between the wavelength of the He II Lα line at $\lambda 303.78$ and the O III $2p^2\,^3P_2$–$3d\,^3P_2^o$ line at $\lambda 303.80$. As we have seen, in the He^{++} zone of a nebula there is some residual He$^+$, so the He II Lα photons emitted by

recombination are scattered many times before they escape. As a result, there is a high density of He II Lα photons in the He^{++} zone, and since O^{++} is also present in this zone, some of the He II Lα photons are absorbed by it and excite the $3d\ ^3P_2^o$ level of O III. This level then quickly decays by a radiative transition, most frequently (relative probability 0.74) by resonance scattering in the $2p^2\ ^3P_2$–$3d\ ^3P_2^o$ line—that is, by emitting a photon. The next most likely decay process (probability 0.24) is emission of $\lambda 303.62\ 2p^2\ ^3P_1$–$3d\ ^3P_2^o$, which may then escape or may be reabsorbed by another O^{++} ion, again populating $3d\ ^3P_2^o$. Finally (probability 0.02), the $3d\ ^3P_2^o$ level may decay by emitting one of the six longer wavelength photons $3p\ ^3L_J$–$3d^3P_2^o$ indicated in Figure 4.6. These levels $3p\ ^3L_J$ then decay to $3s$ and ultimately back to $2p^2\ ^3P$, as shown in the figure (or to $2p^3$ and then back to $2p^2\ ^3P$, emitting two far-ultraviolet line photons, as shown in the figure). This is the Bowen resonance-fluorescence mechanism, the conversion of He II Lα to those lines that arise from $3d\ ^3P_2^o$ or from the levels excited by its decay. These lines are observed in many planetary nebulae, and their interpretation, requiring the solution of the problem of the scattering, escape, and destruction of He II Lα with the complications introduced by the O^{++} scattering and resonance fluorescence, has been worked out years ago. Some of the most important references to it are given at the end of the chapter for those who wish to study it further.

A second accidental near-coincidence occurs between the wavelength of the H I Lβ line at $\lambda 1025.72$ Å and the O I $2p^4\ ^3P_2 - 2p^33d\ ^3D_3^o$ line at $\lambda 1025.76$ Å, which excites the $2p^33d\ ^3D_3^o$ level. Some atomic oxygen exists in the H$^+$ zone, due to rapid charge transfer between oxygen and hydrogen, so the situation is analogous to that for O III and He II Lα. Excitations of $2p^33d\ ^3D_3^o$ by this process are followed by successive decays producing $2p^33p\ ^3P_2$–$2p\ ^33d\ ^3D_3^o\ \lambda 11286.9$ Å, $2p^3\ 3s\ ^3S_1\ ^o$–$2p\ ^33p\ ^3P_2\ \lambda 8446.36$ Å, and the three lines of the multiplet $2p^4\ ^3P_{2,1,0}$–$2p^3\ 3s\ ^3S_1^o \lambda\lambda 1302.17,\ 1304.86,\ 1306.03$ Å. In the simplest case each excitation produces a cascade through the first two of these lines, followed by one of the last three, in the predicted ratio of their transition probabilities, 3.4:2.0:0.7. The relative intensities of the first two lines and the sum of the intensities of the multiplet are thus all equal in photon units, so their predicted relative intensities in energy units are inversely proportional to their wavelengths.

4.8 Collisional Excitation in He I

Collisional excitation of H is negligible in comparison with recombination in populating the excited levels in planetary nebulae and H II regions, because the threshold for even the lowest level, $n = 2$ at 10.2 eV, is large in comparison with the thermal energies at typical nebular temperatures. This can be confirmed quantitatively using collision strengths listed in Table 3.16. However, in He^0 the $2\ ^3S$ level is highly metastable, and collisional excitation from it can be important, particularly in exciting $2\ ^3P^o$ and thus leading to emission of He I $\lambda 10830$ Å. To fix our ideas, let us consider a nebula sufficiently dense ($n_e \gg n_c$) that the main mechanism for depopulating $2\ ^3S$ is collisional transitions to $2\ ^1S$ and $2\ ^1P^o$, as explained in Section 2.4. The
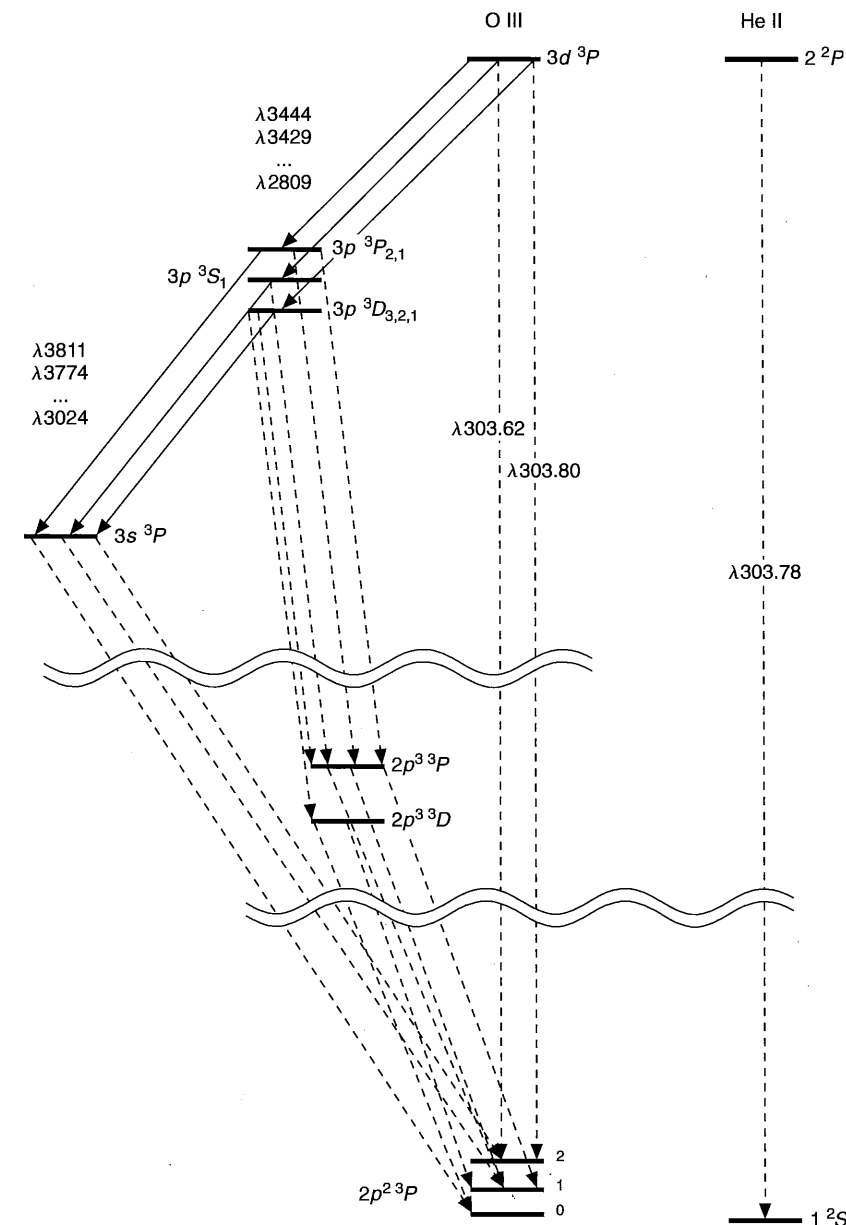
Figure 4.6

Schematized partial energy-level diagrams of [O III] and He II showing coincidence of He II Lα and [O III] $2p^2\ ^3P_2$–$3d\ ^3P\lambda 303.80$. The Bowen resonance fluorescence lines in the optical and near-ultraviolet are indicated by solid lines, and the far-ultraviolet lines that lead to excitation or decay are indicated by dashed lines. There are six observable lines in all leading down from $3d\ ^3P_2^o$, and 14 from $3p\ ^3P_{2,1}$, $3p\ ^3S_1$, and $3p\ ^3D_{3,2,1}$, and with relative strengths that can be calculated just from the ratios of transition probabilities.

Table 4.13

Collision strengths Υ for collisions from $He^0(2\,^3S)$

T (K)	$2\,^3S, 2\,^3P^o$	$2\,^3S, 3\,^3S$	$2\,^3S, 3\,^3P^o$	$2\,^3S, 3\,^3D$	$2\,^3S, 3\,^1D$
6,000	16.3	2.40	1.61	1.46	0.249
10,000	25.8	2.29	1.61	1.95	0.259
15,000	37.1	2.25	1.59	2.52	0.257
20,000	46.5	2.26	1.57	2.99	0.252
25,000	55.3	2.31	1.56	3.43	0.245

equilibrium population in $2\,^3S$ is then given by the balance between recombinations to all triplet levels, which eventually cascade down to $2\,^3S$, and collisional depopulation of $2\,^3S$,

$$n_e n(He^+)\alpha_B(He^0, n^3L) = n_e n(2\,^3S)\left[q_{2\,^3S,2\,^1S} + q_{2\,^3S,2\,^1P^o}\right]. \quad (4.58)$$

The rate of collisional population of $2\,^3P^o$ is thus

$$n_e n(2\,^3S)q_{2\,^3S,2\,^3P^o} = \frac{n_e n(He^+)q_{2\,^3S,2\,^3P^o}}{\left[q_{2\,^3S,2\,^1S} + q_{2\,^3S,2\,^1P^o}\right]}\alpha_B(He^0, n^3L) \quad (4.59)$$

so the relative importance of collisional to recombination excitation of $\lambda10830$ is given by the ratio

$$\frac{n_e n(2\,^3S)q_{2\,^3S,2\,^3P^o}}{n_e n(He^+)\alpha_{\lambda10830}^{eff}} = \frac{q_{2\,^3S,2\,^3P^o}}{\left[q_{2\,^3S,2\,^1S} + q_{2\,^3S,2\,^1P^o}\right]}\frac{\alpha_B(He^0, n\,^3L)}{\alpha_{\lambda10830}^{eff}} \quad (4.60)$$

Computed values for the collision strengths Υ that are used to compute $q_{2\,^3S,2\,^3P^o}$ are listed in Table 4.13; they are much larger than those for $q_{2\,^3S,2\,^1S}$ and $q_{2\,^3S,2\,^1P^o}$ (listed in Table 2.5), because the cross section for the strong allowed $2\,^3S\text{–}2\,^3P$ transition is much larger than the exchange cross sections to the singlet levels. At a representative temperature $T = 10,000$ K, the first factor in Equation (4.60) has the numerical value 6.0; the second, 1.4; and the ratio of collisional to recombination excitation is thus about 8. In other words, collisional excitation from $2\,^3S$ completely dominates the emission of $\lambda10830$, and the factor by which it dominates depends only weakly on T, and can easily be seen to decrease with n_e below n_c.

Though the collisional transition rates from $2\,^3S$ to $2\,^1S$ and $2\,^1P^o$ are smaller than to $2\,^3P^o$, the recombination rates of population of these singlet levels are also smaller, and the collisions are therefore also important in the population of $2\,^1S$ and $2\,^1P^o$. The cross sections for collisions to the higher singlets and triplets are smaller but not negligible; from the best available cross sections it appears likely that collisional population of $3\,^3P^o$ is significant and somewhat affects the strength of $\lambda3889$. The available atomic data indicates that there is a non-negligible collisionally excited
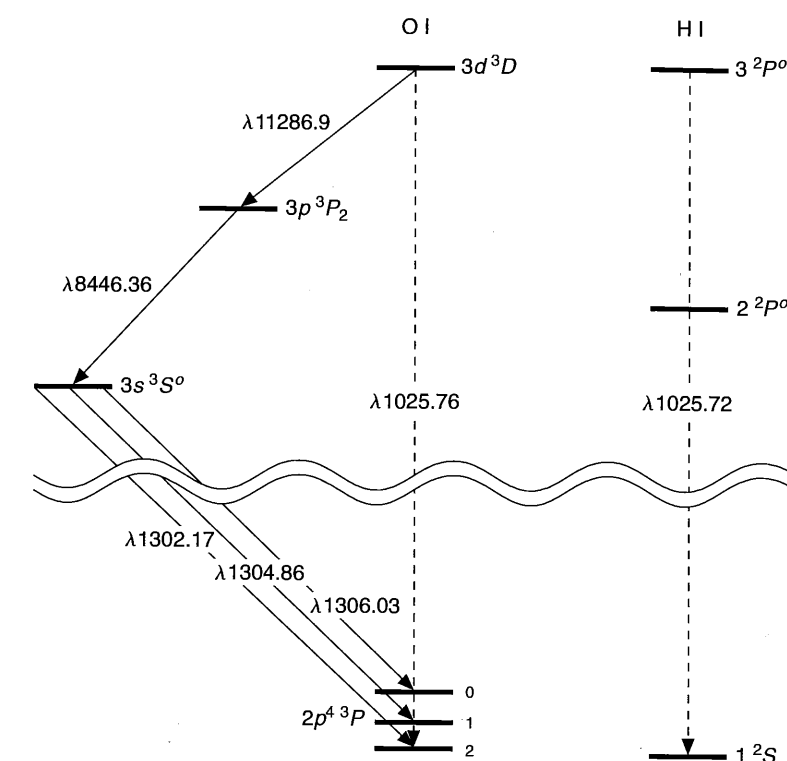
Figure 4.7

Schematized partial energy-level diagrams of O I and H I showing the coincidence between H I Lβ and O I $2p^4\,^3P_2\text{–}2p^33d\,^3D_3^o\lambda1025.76$. The far ultraviolet lines that lead to excitation are indicated by dashed lines, and the cascade lines in the infrared, optical, and ultraviolet are indicated by solid lines.

component in the observed strength of $\lambda5876$ in planetary nebulae. Some collision strengths for the excitation of He I levels with $n = 3$ are also listed in Table 4.13.

Similar collisional-excitation effects occur from the metastable $He^0\,2\,^1S$ and $H^0\,2\,^2S$ levels, but they decay so much more rapidly than $He^0\,2\,^3S$ that their populations are much smaller and the resulting excitation rates are negligibly small.

References

A good general summary of the emission processes in gaseous nebulae is given by

Seaton, M. J. 1960, Reports on Progress in Physics 23, 313.

The theory of the recombination-line spectrum of H I goes back to the early 1930s and was developed in papers by H. H. Plaskett, G. G. Cillie, D. H. Menzel, L. H. Aller, L. Goldberg,

and others. In more recent years it has been refined and worked out more accurately by M. J. Seaton, A. Burgess, R. M. Pengelly, M. Brocklehurst, D. G. Hummer, P. J. Storey, and others. The treatment in Chapter 4 follows most closely the following definitive references:

Seaton, M. J. 1959, MNRAS, 119, 90.

Pengelly, R. M. 1964, MNRAS, 127, 145.

The second reference treats the low-density limit for H I and He II in detail. (Tables 4.1, 4.2, and 4.3 are derived from it.)

Pengelly, R. M., & Seaton, M. J. 1964, MNRAS, 127, 165.

The effects of collisions in shifting L at fixed n are discussed in this reference. Table 4.10 comes from it.

Brocklehurst, M. 1971, MNRAS, 153, 471.

Hummer, D. G., & Storey, P. J. 1987, MNRAS, 224, 801.

Hummer, D. G., & Storey, P. J. 1992, MNRAS, 254, 277.

Storey P. J., & Hummer D. G. 1995, MNRAS, 272, 41 (on the web at *http://adc.gsfc .nasa.gov/adc-cgi/cat.pl?/catalogs/6/6064/*.

These references include the definitive results for H I and He II at finite densities in the optical region, taking full account of the collisional transitions. Tables 4.4 and 4.5 are based upon the last reference, which includes full electronic access.

Robbins, R. R. 1968, ApJ, 151, 497; and ApJ, 151, 511.

Robbins, R. R. 1970, ApJ, 160, 519.

Robbins, R. R., & Robinson, E. L. 1971, ApJ, 167, 249.

Brocklehurst, M. 1972, MNRAS, 157, 211.

Ferland, G. J. 1980, MNRAS, 191, 243.

Almog, U., & Netzer, H. 1989, MNRAS, 238, 57.

Smits, D. P. 1996, MNRAS, 278, 683.

Kingdon, J. B., & Ferland, G. J. 1996, MNRAS, 282, 723.

Hummer, D. G., & Storey, P. J. 1998, MNRAS, 297, 1073.

Porter, R. L., Bauman, R. P., Ferland, G. J., & MacAdam, K. B. 2005, ApJ, 622,73L.

The first two papers by Robbins work out the theory in detail for the He I triplets; the third is concerned with the singlets (for Case A only). The paper by Ferland analyzes the applicability of Case B to the He I singlets. The Porter et al. article is complete, for it describes triplet and singlet results, including collisions from $2\,^3S$. (Table 4.6 is based on it.)

Brown, R. L., & Mathews, W. G. 1970, ApJ, 160, 939.

This reference collects previous references and material on the H I and He II continuum, and includes the most detailed treatment of the He I continuum. (Tables 4.7–4.9 and 4.11 are taken from this reference.)

Ferland, G. J. 1980, PASP, 92, 596.

Martin, P. G. 1988, ApJS, 66, 125.

These references give the continuous spectrum of the H I continuum (for specific wavelengths and filters), and recombination coefficients for Cases A and B over a very wide range in temperature (500 K $\leq T \leq$ 2,000,000 K).

Scheuer, P. A. G. 1960, MNRAS120, 231.

Hummer, D. G. 1988, ApJ, 327, 477.

The first is a very complete reference on free–free emission in the radio-frequency region, while the rest do the general problem.

The first published prediction that the radio-frequency recombination lines of H I would be observable was made by

Kardashev, N. S. 1959, Astron. Zhurnal, 36, 838 (English translation, 1960, Soviet Astronomy AJ, 3, 813.

The key reference on the importance of maser action and on the exact variation of b_n with n is

Goldberg, L. 1966, ApJ, 144, 1225.

The radiative transfer treatment in this chapter essentially follows this reference.

The equilibrium equations for the populations of the high levels are worked out in

Seaton, M. J. 1964, MNRAS, 127, 177.

Sejnowski, T. J., & Hjellming, R. H. 1969, ApJ, 156, 915.

Brocklehurst, M. 1970, MNRAS, 148, 417.

The last of these three references is the definitive treatment and makes full allowance for all collisional effects. (Figure 4.2 is based on it.)

A good deal of theoretical work has been done by several authors on radiative transfer problems in nebulae. The portion of this research used in this chapter is summarized (with complete references) in

Osterbrock, D. E. 1971, JQSRT, 11, 623.

Some of the key references concerning the H I lines are

Capriotti, E. R. 1964, ApJ, 139, 225, and 140, 632.

Capriotti, E. R. 1966, ApJ, 146, 709.

Cox, D. P., & Mathews, W. G. 1969, ApJ, 155, 859.

(Figure 4.3 is based on the last reference.)

The radiative transfer problem of He I lines was worked out earlier in

Pottasch, S. R. 1962, ApJ, 135, 385.

Robbins, R. R. 1968, ApJ, 151, 511.

A more recent treatment is

Almog, U., & Netzer, H. 1989, MNRAS, 238, 57.

(Figure 4.5 is derived from calculations from these references.)

The Bowen resonance-fluorescence mechanism was first described by

Bowen, I. S. 1924, ApJ, 67, 1.

The radiative transition probabilities necessary for tracing all the downward radiative decays following excitation of O III and $3d\ ^3P_1^0$ are given by

Saraph, H. E., & Seaton, M. J. 1980, MNRAS, 193, 617.

Bhatia, A. K., & Kastner, S. O. 1993, ADNDT, 54, 133.

Froese Fischer, C. 1994, Phys. Scripta, 49, 51.

Solutions are described in

Weymann, R. J., & Williams, R. E. 1969, ApJ, 157, 1201.

Harrington, J. P., 1972, ApJ, 176, 127.

Kallman, T., & McCray, R. 1980, ApJ, 242, 615.

Elitzur, M., & Netzer, H. 1985, ApJ, 291, 646.

Netzer, H., Elitzur, M., & Ferland, G. J. 1985, ApJ, 299, 752.

Kastner, S. O., & Bhatia, A. K. 1996, MNRAS, 279, 1137.

Observations of the lines in various objects are described by

Grandi, S. A. 1980, ApJ, 238, 10.

Liu, X.-w., & Danziger, J. 1993, MNRAS 261, 463, and 262, 699.

O'Dell, C. R., & Miller, C. O. 1992, ApJ, 390, 219.

Rudy, R. J., Mazuk, S., Puetter, R. C., & Hamann, F. 2000, ApJ, 539, 166.

The He I collision strengths listed in Table 4.13 are from

Bray, I., Burgess, A., Fursa, D. V., & Tully, J. A. 2000, A&AS, 146, 481.

5

Comparison of Theory with Observations

5.1 Introduction

In the preceding three chapters much of the available theory on gaseous nebulae has been discussed, so that we are now in a position to compare it with the available observations. The temperature in a nebula may be determined from measurements of ratios of intensities of particular pairs of emission lines—those emitted by a single ion from two levels with considerably different excitation energies. Although the relative strengths of H recombination lines vary only extremely weakly with T, the ratio of the intensity of a line to the intensity of the recombination continuum varies more rapidly and can be used to measure T. Further information on the temperature may be derived from radio observations, combining long- and short-wavelength continuum observations (large and small optical depths, respectively) or long-wavelength continuum and optical-line observations. The electron density in a nebula may be determined from measured intensity ratios of other pairs of lines—those emitted by a single ion from two levels with nearly the same energy but with different radiative-transition probabilities. Likewise, measurements of relative strengths of the radio recombination lines give information on both the density and the temperature in nebulae. These methods, as well as the resulting information on the physical parameters of characteristic nebulae, are discussed in the first sections of this chapter.

In addition, information on the involved stars that provide the ionizing photons may be derived from nebular observations. For, if a nebula is optically thick to a particular type of ionizing radiation (for instance, in the H Lyman continuum), then the total number of photons of this type emitted by the star can be determined from the properties of the nebula. By combining these nebular observations, which basically measure the far-ultraviolet-ionizing radiation from the involved stars, with optical measurements of the same stars, a long base-line color index that gives information on the temperature of the stars can be determined. This scheme and the information